Journal of Catalysis **209,** 480–488 (2002)
doi:10.1006/jcat.2002.3631

Extraframework Aluminum Species in Zeolites: Ab Initio Molecular Dynamics Simulation of Gmelinite

L. Benco,*,†,[1] T. Demuth,* J. Hafner,* F. Hutschka,‡ and H. Toulhoat§

*Institut für Materialphysik and Center for Computational Materials Science, Universität Wien, Sensengasse 8, A-1090 Vienna, Austria; †Institute of Inorganic Chemistry, Slovak Academy of Sciences, Dubravska cesta 9, SK-84236 Bratislava, Slovakia; ‡Totalfinaelf, Centre Européen de Recherche et Technique, B.P. 27, F-76700 Harfleur, France; and §Institut Français du Pétrole, F-92852 Rueil-Malmaison Cedex, France

Received January 22, 2002; revised April 4, 2002; accepted April 4, 2002

The dynamical behavior of extraframework aluminum particles (EFAL) in zeolites has been investigated using a first-principles molecular dynamics technique. Small clusters of hydrated aluminum hydroxide $Al(OH)_3(H_2O)_3$ and $Al(OH)_3(H_2O)$ are located both in the main channel and in the cage. The simulation of the hexacoordinated cluster at $T = 300$ K shows an overcoordination of the central atom and a release of H_2O molecules. When placed in the main channel both the EFAL and the noncoordinated H_2O molecules are mobile. When placed in the cage, a network of hydrogen bonds is established, occluding the EFAL and suppressing its mobility. The basic character of the EFAL causes an exchange of Brønsted acid protons between the zeolite and the EFAL particle. In a high-acidity zeolite a multiple, simultaneous proton exchange is observed, leading to a separation of charges ($EFAL^{2+}$, $zeolite^{2-}$). The calculated stretching OH frequencies of the EFAL are ~ 60 cm^{-1} higher than those of the Brønsted OH, in good agreement with IR measurements.

1. INTRODUCTION

The large internal surfaces of zeolites act as strong sorbents and their micropores always contain particles of various kinds and origin. These particles are either deposited via adsorption from the atmosphere or originate from the zeolite structure itself. Extraframework aluminum (EFAL) represents part of the structure released upon the hydrothermal steaming or acid leaching used to adjust the Si/Al ratio in the framework. The nature of EFAL particles has been the subject of many investigations and two forms have been proposed (1): cationic particles adsorbed in anionic zeolites (Al^{3+}, AlO^+, $Al(OH)^{2+}$, $Al(OH)_2^+$) and neutral or polymerized forms ($AlO(OH)$, $Al(OH)_3$, Al_2O_3).

Because the presence of EFAL can influence both the catalytic and the transport properties of zeolites, the EFAL particles have been characterized by various experimental techniques. ^{27}Al MAS NMR has been widely used to characterize the local environment of Al. Four-, five-, and sixfold coordination of Al has been suggested (2–5). The locations of EFAL have been studied by X-ray and neutron diffraction (6, 7). The relative abundance of different types of EFAL and their reactivity with different reagents has been investigated by Gola *et al.* (8). EFAL species are characterized as hydroxylated particles producing a well-resolved IR stretching band. The band of the zeolite Brønsted H atoms is observed at 3610–3620 cm^{-1}, and the band of external silanol groups is located at $\sim$3740 cm^{-1}. The hydroxyl groups of the EFAL species produce a band at $\sim$3670 cm^{-1} (9, 10).

In order to sample the behavior of the EFAL particles we performed a series of dynamical simulations of small hydroxylated Al clusters located in the zeolite. The bonding in the most abundant forms, tetra- and hexacoordinated aluminum, is compared with that of free nonadsorbed particles. The dynamical behavior of particles in the zeolite is probed for different locations of EFAL. Finally, the hydrogen bonding of the EFAL particle to the zeolite framework is compared for two different concentrations of the acid sites of the zeolite.

2. STRUCTURAL MODEL

The simulation of the EFAL particles in the zeolite is performed for gmelinite. Purely siliceous gmelinite has the composition $Si_{24}O_{48}$ and forms a hexagonal structure with space group $P6_3mmc$. The cell dimensions are $a = b = 13.756$ Å and $c = 10.048$ Å (11). The secondary building block of the gmelinite structure is a hexagonal prism. The stacking of building blocks leads to a columnar structure, with prisms and gmelinite cages alternating along each column (see Fig. 1). The largest channel is circumscribed by a ring of 12 SiO_4 tetrahedra (the 12-membered ring—12MR) extending along one dimension (the c-axis).

Gmelinite is good candidate for ab initio simulations of intrazeolite phenomena. In previous studies we used the structure of gmelinite to characterize Brønsted acid sites

[1] To whom correspondence should be addressed. Fax: +43-1-4277-9413. E-mail: lubomir.benco@univie.ac.at.

0021-9517/02 $35.00

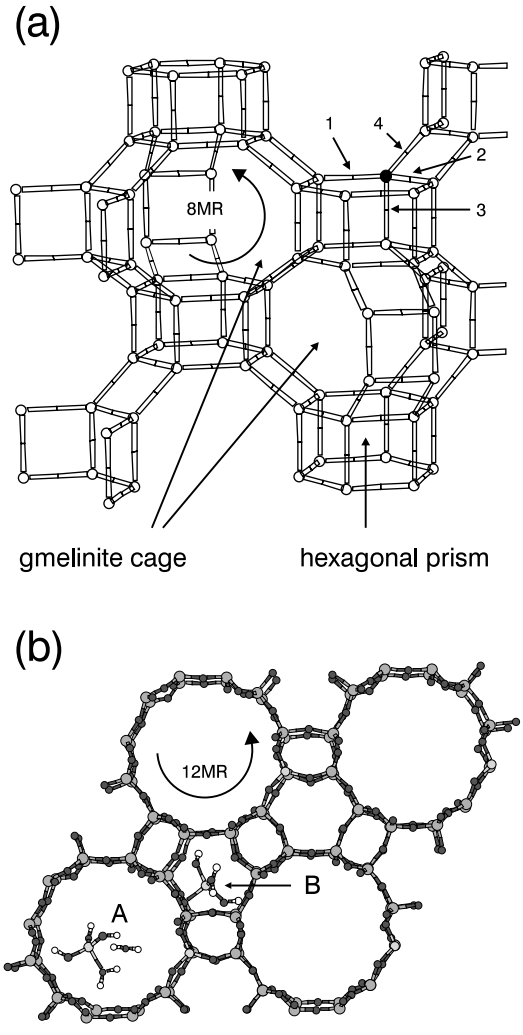

FIG. 1. Hexagonal structure of gmelinite. (a) The framework structure. (b) Top view showing the large 12MR channels. Two locations of the EFAL particle are (A) in the main channel or (B) in the gmelinite cage.

(12), spontaneous proton transfer (13, 14), ion-exchange and hydration processes (15), and adsorption of linear hydrocarbons (16). Recently Dura-Vila and Gale simulated palladium clusters immobilized in the gmelinite structure (17).

The structure contains both large channels and relatively small cavities. The gmelinite cage and the hexagonal prism also constitute elements of the crystal structure of faujasites, which are industrially important zeolites. The kinetic diameter of the main channel of ~7 Å is comparable with those of the large-pore zeolites. Due to the high space group symmetry all tetrahedral sites (Si/Al) are crystallographically equivalent and there are only four inequivalent O sites (numbered 1 to 4 in Fig. 1a). The rather uniform shape of the unit cell allows the insertion of relatively large particles, such as the hexane molecule (16).

The simulation of EFAL particles is done with the experimental unit-cell parameters (11). The X-ray structure determination has been performed on natural gmelinite with a Si/Al ratio of approximately 2/1. The samples contain the corresponding number of counterions and a not very precisely known number of water molecules. The typical composition is $Na_8(AlO_2)_8(SiO_2)_{16} \cdot xH_2O$ ($x = 22$–24). The experimental lattice vectors $a = b = 13.756$ Å and $c = 10.048$ Å (11) thus correspond to a unit cell slightly expanded due to the hydration. An additional expansion is expected for structures containing EFAL particles adsorbed in the large pores or occluded in the gmelinite cage. The experimental unit-cell volume of the hydrated zeolite corresponds reasonably well with the optimized volume of the EFAL-anchoring zeolite.

^{27}Al MAS NMR indicates that the most abundant forms of the EFAL particles are tetra- and hexacoordinated species (8). An admixture of the pentacoordination in fresh samples disappears upon a leaching treatment. In our simulations we use the two most stable forms of clusters, the tetra- and hexacoordinated particles. The clusters are derived from neutral aluminum hydroxide in which the coordination number is increased by the insertion of H_2O molecules. Only mononuclear particles are used. The cluster with the composition $Al(OH)_3(H_2O)_3$ thus represents the six-coordinated Al atom with a bonding similar to that of the structure of boehmite (18) and $Al(OH)_3(H_2O)$ represents the neutral particle with a four-coordinated Al atom. In the zeolite structure the particles are placed either in the main channel or into the gmelinite cage (cf. Fig. 1b).

3. COMPUTATIONAL DETAILS

Ab initio molecular dynamics simulations have been performed to characterize the structural and dynamical properties of both the zeolite and the EFAL particle. The calculations are based on density-functional theory (19) using the generalized-gradient approximation (20) to the exchange-correlation functional. The calculations are performed using Blöchl's projector augmented wave (21, 22) technique applied to ultrasoft pseudopotentials (23, 24). We use a plane–wave basis as implemented in the Vienna ab initio simulation package VASP (25). The plane–wave cutoff energy is 300 eV for the molecular dynamics and 400 eV for the static relaxation of structures. The relatively large dimensions of unit cells of zeolites enable a restriction of the Brillouin-zone sampling to the Γ point. Convergence is improved using a modest smearing of the eigenvalues. The Gaussian-like partial occupancies of energy levels are introduced around the Fermi level, and the total energy is extrapolated to the zero smearing. The relaxation of structures is performed via a conjugate-gradient algorithm until differences of the total energies are converged below 10^{-4} eV. Fixed-volume molecular dynamics simulations are

performed at 300 K. The dynamics uses the exact Hellman–Feynman forces acting on atoms and applies the statistics of the canonical ensemble to the motion of atomic nuclei (26) and the Verlet velocity algorithm (27) with a time step for the integration of equations of motion of $\Delta t = 1.0$ fs. The frequency bands are calculated via the Fourier transform of the velocity autocorrelation function. The simulation time is 2 ps. The frequency of the heat bath is tuned to that of the O–H stretching to support the mobility of the acid proton.

4. RESULTS AND DISCUSSION

In the dynamical simulation a full ab initio calculation of the electronic ground state of the zeolite containing the EFAL particle is performed at each time step. All types of interactions are thus considered for the zeolite framework, the EFAL particle, and the EFAL-to-zeolite interactions. Bonding within small EFAL particles, however, is influenced by external interactions with the zeolite framework. For the sake of comparison we first evaluate the structures of the EFAL clusters *in vacuo*.

4.1. EFAL Particles In Vacuo

The relaxed structures of the clusters $Al(OH)_3(H_2O)_3$ and $Al(OH)_3H_2O$ are displayed in Fig. 2. The relaxation of the cluster of the six-coordinated Al atom (Fig. 2a) is initiated from the quasioctahedral arrangement with two water molecules in the axial positions and three hydroxyl groups and one water molecule in the equatorial position (not displayed). The relaxation leads to a decrease in the coordination of the central atom and to the rotation of the water molecules in such a way that a maximum number of hydrogen bonds is established (dotted lines in Fig. 2a). The coordination of the central Al atom decreases from six to five. One water molecule, formerly connected in the equatorial position, is pushed out of the octahedron and placed at a Al–O distance of ~4 Å. The Al atom thus becomes only pentacoordinated. The expelled water molecule connects to one of the OH groups via a hydrogen bond. The H . . . O distance of 1.934 Å indicates that hydrogen bonding of this excess molecule is weak (28). The bond distances of the two water molecules connected to the central atom are 2.049 and 2.136 Å. Much shorter distances of the three hydroxyl groups of 1.741, 1.747, and 1.782 Å, respectively, indicate a stronger bonding of the OH^- groups compared with that of the neutral H_2O molecules. Similarly, the O–H distances in the hydroxyl groups 0.962, 0.962, and 9.966 Å are shorter than the O–H distances in water molecules. Remarkably, the O–H distance in the O–H groups of the water molecules involved in hydrogen bonds is considerably longer (cf., e.g., the O–H bond length 0.993 Å).

The bonding in the tetracoordinated Al particle (Fig. 2b) show similar features. The decrease in the coordination number, however, induces a stronger bonding, leading to shorter Al–O distances compared with the hexa-/pentacoordinated particle (Fig. 2a). The water molecule is connected at a distance of 2.00 Å. The strengthening of the coordination prevents a rotation of the molecule and the formation of hydrogen bonds to the O–H groups. While the Al–O distances of the O–H groups are slightly shorter than those in the hexa-/pentacoordinated particle, the O–H bond lengths of 0.965 Å remain similar.

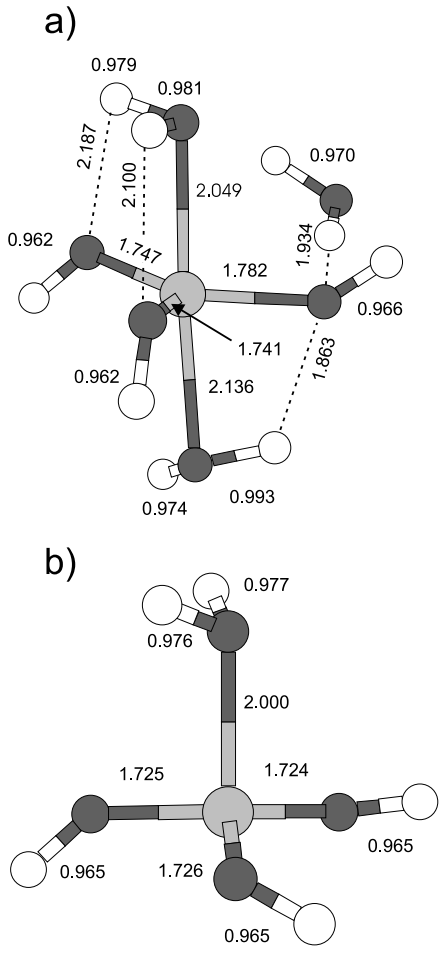

FIG. 2. Geometries of EFAL particles relaxed *in vacuo*. (a) Hexacoordinated $Al(OH)_3(H_2O)_3$. (b) Tetracoordinated $Al(OH)_3H_2O$. The numbers are bond distances in angstroms. Dashed lines indicate intracluster hydrogen bonds. In the hexacoordinated particle one water molecule is expelled out to the second coordination sphere.

The comparison of the bonding in $Al(OH)_3(H_2O)_3$ and $Al(OH)_3H_2O$ shows a rather loose bonding of the water molecules in both hexa- and pentacoordinated clusters. A release of one water molecule is observed in the hexacoordinated particle, and within the pentacoordinated configuration rotations of water molecules lead to intraparticle hydrogen bonds. On the other hand, the bonding in the tetracoordinated particle is stronger, the bond distances are shorter, and no hydrogen bonds are established in the relaxed structure.

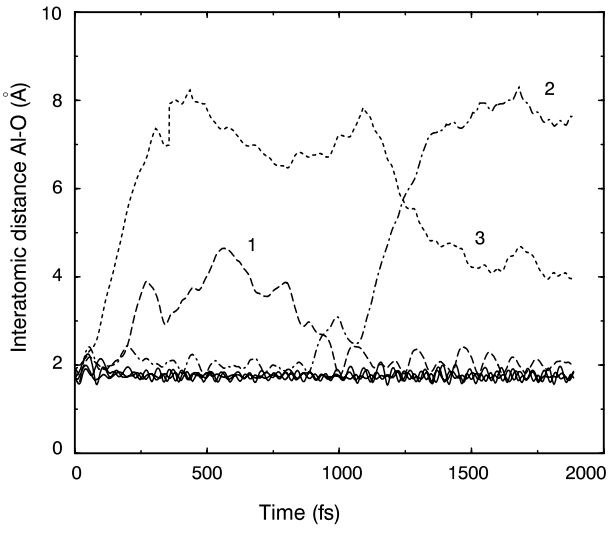

FIG. 3. Interatomic distances Al–O of the six-coordinated Al atom. The coordination sphere consists of three OH groups and one water molecule. One H_2O molecule is loosely coordinated at a distance of ∼4 Å and one molecule resides at a distance of ∼7 Å.

4.2. Hexacoordinated EFAL in the Main Channel

The room temperature simulation is performed with the $Al(OH)_3(H_2O)_3$ cluster placed in the main channel of the zeolite (cf. position A in Fig. 1b). The low-Al zeolite contains one Al atom per cell with one Brønsted acid acid site (AS) at the O4 position of the zeolite framework oriented into the main channel. Figure 3 shows the time evolution of the Al–O interatomic distances. Three solid lines are used for the Al–O distances of the hydroxyl groups and broken lines (labeled 1–3) for those of the water molecules. The fluctuation of the bond lengths of the hydroxyl groups is small, of the order 0.2–0.3 Å. This corresponds with the strong bonding of the hydroxyl groups and short interatomic distances in the relaxed structures (Fig. 2). Of the three water molecules, one remains close to the Al atom. In the time interval from 0 to ∼1000 fs, this is the molecule labeled 2 in Fig. 3; in the time interval from 1000 to 2000 fs, this is the molecule labeled 1. The other two molecules move to rather large distances of ∼4 and ∼7 Å, respectively. Here again we observe a spontaneous rearrangement. As molecule 2 is detached from the Al atom, it quickly moves to a distance of ∼7 Å, while molecule 3 approaches up to a distance of ∼4 Å. The shorter distance of ∼4 Å, corresponds to the loosely connected water molecule in the overcoordinated cluster in Fig. 2a. The distance of ∼7 Å corresponds to a molecule not directly connected to the EFAL particle. Because EFAL is situated in the main channel of the zeolite, the distance of ∼7 Å corresponds to a location of the water molecule in the gmelinite cage.

Figure 4 shows the final position of the hexacoordinated EFAL particle inside the main channel of gmelinite. Two replicas of EFAL in two neighboring channels, A and B, from the infinite number of images within the periodical approach are displayed. Two replicas of water molecules 1–3 are displayed as well. For the two most mobile molecules, 2 and 3, Fig. 4 shows the full trajectory of the O atom and the starting and the final location of the molecule. From the beginning of the simulation up to ∼800 fs water 2 is the most tightly bound molecule (cf. Fig. 3). Empty circles indicate that its location is in the main channel (Fig. 4). The molecule is then detached from the EFAL particle and enters the eight-membered ring (8MR) connecting the channel and the gmelinite cage (GC). Then it migrates into the GC and the final location of molecule 2 is inside the GC. Molecule 3 rapidly disconnects from the EFAL particle at the beginning of the simulation (Fig. 3) and moves around inside the GC (cf. Fig. 4). At ∼1200 fs this molecule leaves the GC through the 8MR and approaches the EFAL cluster in the main channel. For the rest of the simulation molecule 3 remains loosely coordinated to the EFAL particle.

The simulation demonstrates that only one water molecule is tightly bound to the aluminum hydroxide particle. The excess water molecules show a high mobility. An interesting feature is that the exchange of positions of water molecules is observed during the simulation. The formerly tightly bound molecule 2 is released by the connection of molecule 1 to the central atom and upon the release of 2 the formerly free molecule 3 becomes coordinated. During

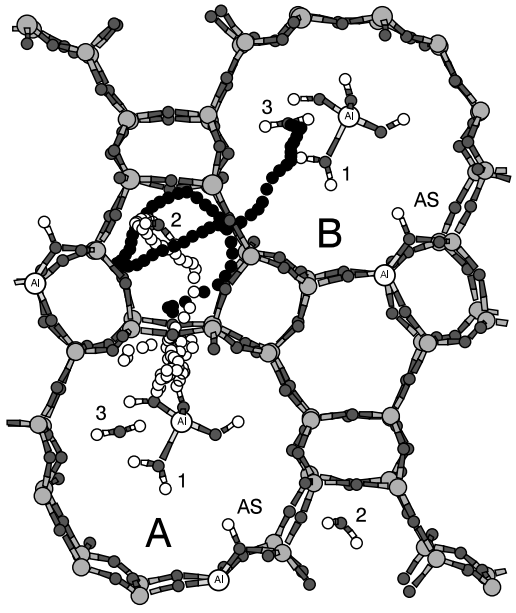

FIG. 4. The dynamics of the EFAL particle $Al(OH)_3(H_2O)_3$ adsorbed in the main channel of the zeolite. The trajectories of the two most mobile water molecules are displayed. Empty circles indicate the diffusion of water from the EFAL particle to the gmelinite cage. The full circles display the diffusion of water from the EFAL through the gmelinite cage to another channel (cf. channels A and B).

the simulation the EFAL particle is mobile. No preferential location at some position within the channel is observed which could be detected by the X-ray diffraction. This is in agreement with measurements of stabilized large-pore Y zeolite by Gola *et al*. (8) detecting no preferred occupancies in the supercage of the steamed solid.

The simulations are performed with the EFAL particle located in the main channel and with one acid site (AS) at the O4 position of the zeolite framework. The water molecule is documented to exhibit considerable affinity toward the AS in zeolites. The adsorption energies of 80–110 kJ/mol are reported for water adsorbed in acid gmelinite (13) and in acid mordenite (29). In the presence of both the EFAL particle and the AS (cf. the location of the EFAL and the AS in Fig. 4) we observe the intercation of the excess water molecules only with the EFAL particle and with the zeolite framework but not with the AS. The adsorption of water on the AS does not occur because of the short duration of the simulation. In the initial arrangement of the EFAL particle the loosely coordinated water molecules are located at that side of the cluster which is oriented toward the zeolite. The contact with the zeolite framework prompts water to move into the gmelinite cage. Because of the absence of any adsorption center inside the zeolite the migrating molecule leaves the framework. Then it makes contact with the EFAL particle because the cluster is located closer to the window of the gmelinite cage. We expect, however, that the final location of the free water molecule in the zeolite is at the acid site.

4.3. Tetracoordinated EFAL in the Gmelinite Cage

A comparison of structures of tetra- and hexacoordinated particles (cf. above) shows that bonding in tetracoordinated particles is more efficient. Strong bonds are formed only between the central atom and the four surrounding O atoms. The simulation of EFAL in the GC is therefore performed with the more compact four-coordinated Al particles. The dimensions of the GC of $\sim 10 \times \sim 6.5$ Å (cf. Fig. 1a) are smaller than those of the main channel. The largest dimension of the relaxed $Al(OH)_3H_2O$ is ~ 5 Å (cf. Fig. 2b). In the GC the four-coordinated EFAL particle can be accommodated without any steric constraints. The apertures separating the GC from the main channel are eight-membered rings (8MR). The dimensions of the 8MR of $\sim 6.3 \times \sim 6.5$ Å are probably not large enough that tetracoordinated particle can leave the cage and move into the main channel. Experiments indicate that the EFAL particles concentrate inside the structure in the secondary pore system (30). The molecular dynamics simulation probes the behavior of EFAL and shows interactions driving the final location of the particle. As particle-to-zeolite interactions can depend on the number of the acid sites, two different concentrations are checked. The starting position of the EFAL particle is chosen inside the gmelinite cage.

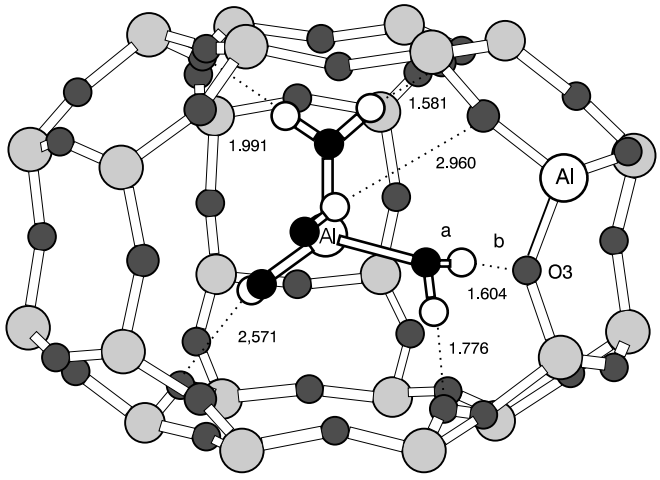

FIG. 5. Geometry of the $Al(OH)_3H_2O$ adsorbed in the gmelinite cage of the zeolite with one acid site. Dotted lines indicate the hydrogen bonds. The acid H atom is transferred from the O3 site of the zeolite to the hydroxyl group of the EFAL particle.

Low concentration of acid sites. The low-Al zeolite is represented by gmelinite containing one acid site per unit cell. Figure 5 shows one of possible positions of the EFAL particle inside the GC of gmelinite. Upon relaxation of the zeolite framework with the EFAL particle a network of the hydrogen bonds (HB) is established. HBs are formed between the hydrogen atoms of both the water molecule and the hydroxyl groups of the EFAL on one side and the oxygen atoms of the zeolite framework on the other side. The calculated adsorption energy of the $Al(OH)_3H_2O$ cluster is 96 kJ/mol. In Fig. 5 the HBs are indicated by dotted lines. The numerical values giving the length of the HB illustrate that a broad spectrum of connections is formed. The shortest connection of 1.58 Å belongs to the category of strong HBs. Several connections with the distances 1.7–2.0 Å represent the hydrogen bonds of the medium strength. Finally, the hydrogen bond distance 2.96 Å is close to the upper limit of the HB of 3.0 Å (28). In the relaxed configuration the acid H atom is transferred from the O3 site of the zeolite to the hydroxyl group of the EFAL particle.

Figure 6 displays the O–H interatomic distances of the acid H atom. The full line (Fig. 6a) shows the distance of the H atom from the oxygen atom of the hydroxyl group of the EFAL particle and the dotted line (Fig. 6b) is the distance of the acid proton from the O3 site of the zeolite (cf. Fig. 5). The time development of the two distances (Fig. 6) shows that the acid H atom of the zeolite is permanently transferred to the EFAL particle. The attachment to the hydroxyl group forms neutral Al-coordinated water molecule (cf. Fig. 5). With the proton transfer a separation of charges occurs, with the positive charge located on the Al atom and the negative charge on the zeolite O atoms, surrounding the Al site. Only for short periods of time does

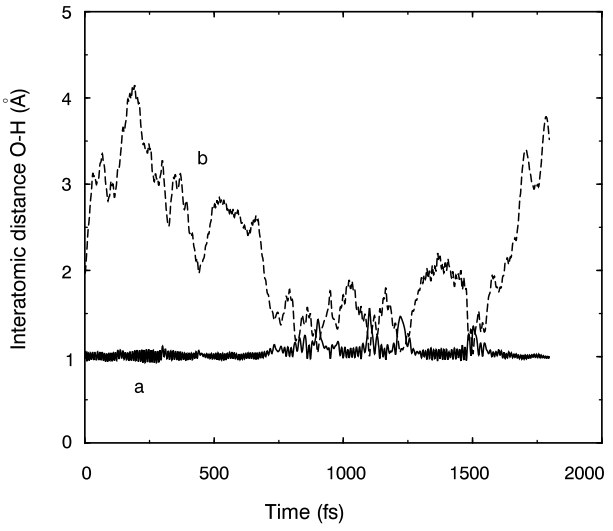

FIG. 6. Time dependence of the O–H interatomic distances. Two lines show the O–H bond length and O–H . . . O hydrogen bond (cf. a and b in Fig. 5). The crossing of the two lines indicates the proton exchange between the EFAL particle and the O3 site of the framework.

the acidic proton jump back to the zeolite (cf. crossing of the two lines in Fig. 6). In spite of numerous hydrogen bonds the acid H atom is the only atom exchanging the position between the zeolite and the EFAL particle. In principle any other H atom of the EFAL particle could be transferred back to some of the O atoms neighboring the Al site. No such event, however, is observed during the short period of simulation.

The network of the HBs considerably suppresses the mobility of the particle and keeps the EFAL in the asymmetric position relative to the center of the GC. During the dynamical equilibration on the time scale of our simulation we observe no change of the position of the EFAL particle. The location (cf. Fig. 5) is in reasonable agreement with noncentered positions of EFAL detected within the sodalite cage of a stabilized Y zeolite (8). Such a location of EFAL in the cage indicates that occluded particles could be as small as a mononuclear Al cluster. The adsorption energies of EFAL and of the water molecule are similar (∼100 kJ/mol). Moreover, both particles interact with the zeolite framework through O–H . . . O hydrogen bonds. We therefore anticipate that in low-Al zeolites the dynamical properties of small particles, such as $Al(OH)_3H_2O$, and of the water molecule are similar. A rearrangement of the HBs between the EFAL particle and the zeolite can lead to a relocation of EFAL within the cage. In any new position, however, the network of HBs will keep the EFAL asymmetrically displaced toward the framework Al atom.

High concentration of acid sites. A high-Al zeolite is produced by six Al/Si substitutions per cell, corresponding to a Si/Al ratio of 3. The positions of Al atoms and the structure of the relaxed tetracoordinated $Al(OH)_3H_2O$ cluster are displayed in Fig. 7. The Al atoms are distributed randomly, leading to rather uniform distribution of the acid sites over the O sites of the zeolite. A fraction of the AS are located directly on the GC and are available for contacts with the EFAL particle. The multiple contacts of the occluded particle with the acid H atoms intensifies the phenomena observed in low-Al zeolite. An effective network of hydrogen bonds is established between the EFAL particle, the acid sites, and the O sites of the zeolite. This network strongly stabilizes the occluded particle. The calculated adsorption energy of 311 kJ/mol is more than three times higher compared with that of the low-Al zeolite (96 kJ/mol). Due to the strong hydrogen bond one acid H atom is permanently transferred to the EFAL (cf. distances a and d in Fig. 7), similarly to low-Al zeolite. Two other strong hydrogen bonds are observed (cf. distances b and e, c and f in Fig. 7). Figure 8 displays the time evolution of the interatomic distances in the three strongest hydrogen bonds. The upper panel shows the distances within the HBs leading to the permanent proton transfer. The acid proton is located at the oxygen atom of the EFAL particle. The bond-distance a varies around ∼1.05 Å. The much larger value compared to ∼0.97 Å of the H_2O molecule in nonoccluded EFAL particles (cf. Fig. 1) indicates the existence of the strong HB toward the framework O site. The crossing of the two lines shows that short-time back transfers of the H atom are observed toward the end of the simulation. This is probably induced by another H transfers from zeolite to the EFAL (cf. another two panels below), leading to a large separation of charges. The back transfer of the H atom thus diminishes the charge separation. The central and bottom panels of Fig. 8 show relatively frequent transfer of another two H atoms from the zeolite framework to the EFAL particle. These transfers are not simultaneous. A simultaneous transfer of two H atoms is detected for short periods of

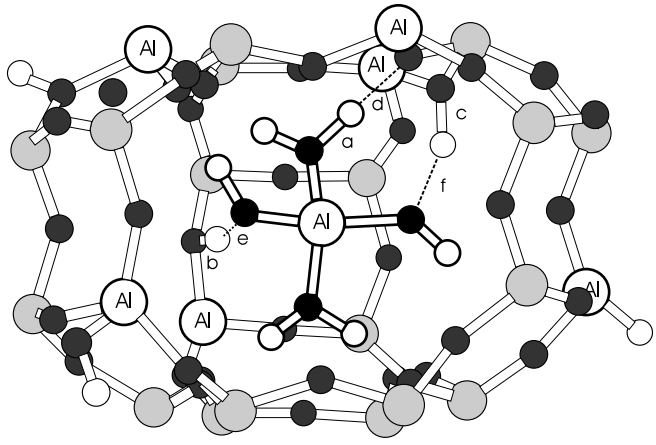

FIG. 7. Geometry of the $Al(OH)_3H_2O$ adsorbed in the gmelinite cage of the zeolite with Si/Al = 3. Dotted lines indicate three strongest hydrogen bonds.

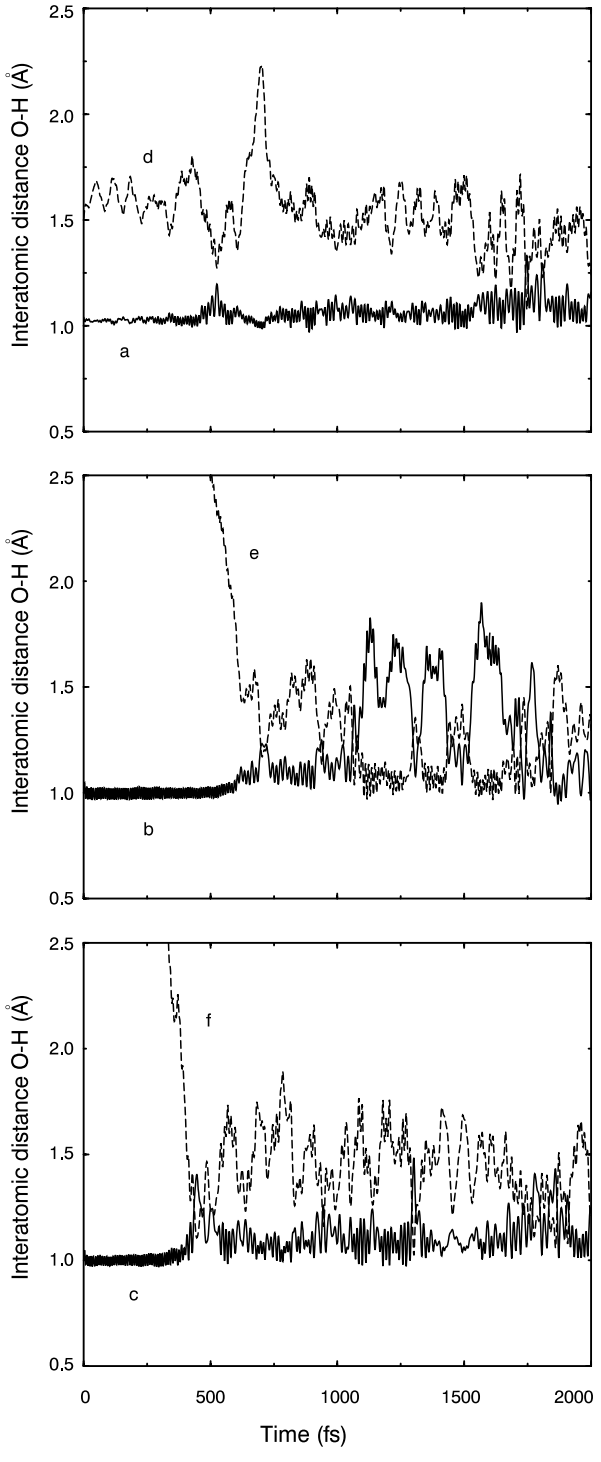

FIG. 8. Time dependence of the O–H interatomic distances of three O–H . . . O contacts of EFAL with acid sites of the high Al zeolite (Si/Al = 3). (a–c) Three O–H bond lengths; (d–f) the corresponding OH . . . O contacts (cf. notation in Fig. 7).

time only, between ∼1700 and ∼1800 fs of the simulation. Parallel with this double transfer, however, the back transfer of the first H atom is observed (cf. the upper panel of Fig. 8). This means that the charge separation between the framework and the occluded particle is limited and does not exceed the values: $EFAL^{+2}$, $zeolite^{-2}$.

IR spectra of the O–H stretching. The bands of vibrational density of states of the high-Al zeolite containing the tetracoordinated EFAL particle are calculated via Fourier transform of the velocity autocorrelation function. The O–H stretching bands, displayed in Fig. 9, are uniformly shifted by ∼240 cm^{-1} to higher frequencies. The spectrum consists of two main bands. The components are projected onto those hydroxyl groups which are not involved in hydrogen bonds. The low-frequency band is found to originate from Brønsted hydroxyl groups and the band at the high-frequency side originates from the O–H groups of the EFAL particle. The separation of the two bands of ∼60 cm^{-1} is in good agreement with experimental data (9, 10). The O–H stretching frequencies of both water molecules and of the hydroxyl groups involved in the HBs do not form any band (Fig. 9d). Relatively narrow bands,

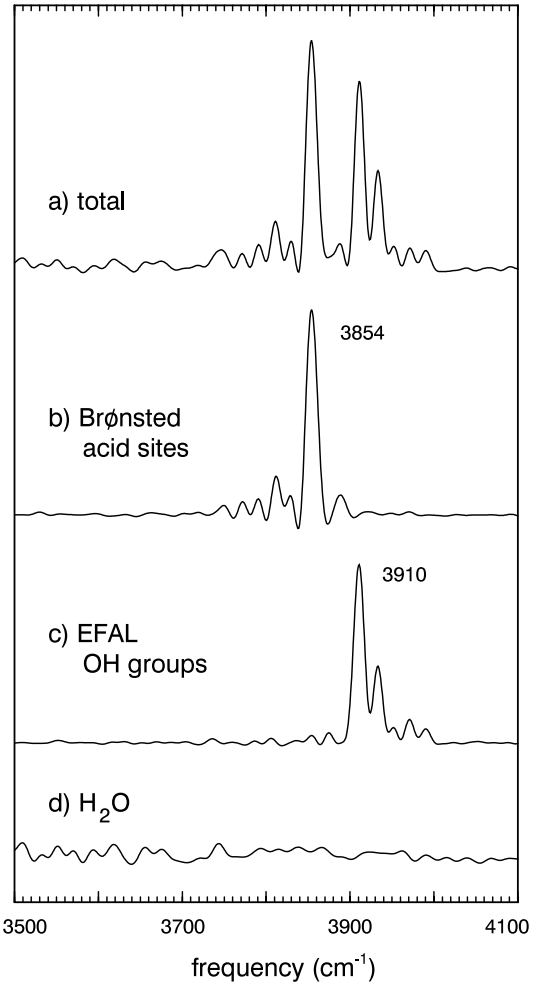

FIG. 9. O–H stretching bands of the acid zeolite (Si/Al = 3) with $Al(OH)_3H_2O$ occluded in the gmelinite cage. (a) Total density of vibrational states. (b–d) H-projected states.

such as those in Figs. 9b and 9c originate from stretching of free nondisturbed O–H bonds. When the hydrogen atom is involved in a hydrogen bonding the stretching frequencies are decreased proportionate to the strength of the HB (28). The frequencies of the hyhrogen-bonded O–H groups could be collected in clear bands if the O–H . . . O connection is stable and without rearrangements, such as detachment from the specific O atom and connection to another atom. The HBs formed between EFAL and the zeolite framework, however, do not represent stable equilibrated bonding connections. Both proton jumps between the two bodies and displacements of the OH groups cause the strength of the hydrogen bonds to vary within a broad interval. The corresponding stretching frequencies are therefore scattered over broad intervals. Due to the short simulation time these frequencies are lost in the background (Fig. 9d). In the long-term simulation we expect appearance of a broad down-shifted band of the hydrogen-bonded hydroxyl groups.

5. CONCLUSIONS

First-principles short-time molecular dynamics simulations have been performed to investigate the structural and dynamical properties of extraframework aluminum particles (EFAL) in a zeolite framework. The EFAL particles are represented by small-size mononuclear clusters of aluminum hydroxide. The coordination number of the central atom is increased via the insertion of neutral H_2O molecules. Two different clusters have been studied. A hexacoordinated Al cluster with the composition $Al(OH)_3(H_2O)_3$ and a tetracoordinated $Al(OH)_3(H_2O)$.

The relaxation of the clusters *in vacuo* shows that in the free $Al(OH)_3(H_2O)_3$ particle the Al atom is overcoordinated. One water molecule is pushed out of the first coordination sphere, thus decreasing the coordination number of the central atom. The bonding in the tetracoordinated cluster, contrarily, is stronger and more compact.

The effect of the interaction of the clusters with the zeolite framework is investigated for $Al(OH)_3(H_2O)_3$ and $Al(OH)_3(H_2O)$ placed in gmelinite. Two different locations are studied: the main channel of the framework and the gmelinite cage. The dynamical simulation of the hexacoordinated cluster at $T = 300$ K located in the main channel shows overcoordination of the Al atom, in agreement with the bonding in the cluster relaxed *in vacuo*. One of the H_2O molecules is completely released and moves through channels and cages of the structure. Another water molecule remains loosely coordinated to the central atom at a distance of ~4 Å. In the main channel both the EFAL and the loosely coordinated H_2O molecules are mobile. The small unbound water molecules diffuse through the zeolite structure via cages and channels. In the gmelinite cage a network of hydrogen bonds between the EFAL particle and the surrounding framework is established, suppressing the mobility of the EFAL. The predicted occlusion of the EFAL is in agreement with experimental observations.

Because of the basic character of the EFAL particle, an exchange of the Brønsted acid H atom occurs between the zeolite framework and the occluded particle. In a high-acidity zeolite a multiple simultaneous proton exchange is observed, leading to the separation of charges ($EFAL^{2+}$, $zeolite^{2-}$). The calculated stretching frequencies of hydroxyls of the EFAL particle are ~60 cm^{-1} higher than those of the Brønsted hydroxyl groups, in good agreement with IR measurements.

Our dynamical simulations demonstrate that in zeolites with occluded EFAL particles a high mobility of the acid protons is observed, caused by the exchange of H atoms between the zeolite framework and the EFAL particle. The exchange is facilitated by a network of hydrogen bonds which strongly stabilize small EFAL particles in the zeolite cage. The first-principles simulations thus provide some details of the microscopic processes taking place inside these complex catalytic systems and increase the understanding of intrazeolite phenomena.

ACKNOWLEDGMENTS

The work was performed within the Groupement de Recherche Européen "Dynamique Moléculaire Quantique Appliquée à la Catalyse," founded by the Conceil National de la Recherche Scientifique (France), the Institut Français du Pétrole (IFP), TOTALFINAELF Recherche et Development, and the Universität Wien. Computing facilities at IDRIS (France) are kindly acknowledged.

REFERENCES

1. Scherzer, J., *in* "Catalytic Materials: Relationship between Structure and Activity" (T. E. White, R. A. Della Betta, E. G. Derouane, and R. T. K. Baker, Eds.), ACS Symp. Ser. 248, p. 157 Am. Chem. Soc., Washington, D.C., 1984.
2. Ray, G. K., Meyers, B. L., and Marshall, C. L., *Zeolites* **7**, 307 (1987).
3. Gilson, J. P., Edwards, G. C., Peters, A. W., Rajagopalan, K., Wormsbecher, R. F., Roberie, T. G., and Shatlock, M. P., *J. Chem. Soc. Chem. Commun.* 91 (1987).
4. Samoson, A., Lippmaa, E., Engelhardt, G., Lohse, U., and Jerschkewitz, H. G., *Chem. Phys. Lett.* **134**, 589 (1987).
5. Ray, G. J., and Samoson, A., *Zeolites* **13**, 410 (1993).
6. Maher, P. K., Hunter, F. D., and Scherzer, J., *in* "Molecular Sieve Zeolites—I, Advances in Chemistry" (R. F. Gould, Ed.), p. 266. Am. Chem. Soc., Washington, D.C., 1971.
7. Parise, J. B., Corbin, D. R., Abrams, L., and Cox, D. E., *Acta Crystallogr. Sect. C* **40**, 1493 (1984).
8. Gola, A., Rebours, B., Milazzo, E., Lynch, J., Benazzi, E., Lacombe, S., Delevoye, L., and Fernandez, C., *Microporous Mesoporous Mater.* **40**, 73 (2000).
9. Corma, A., Corell, C., Fornes, V., Kolodziejski, W., and Perez-Patiente, J., *Zeolites* **15**, 576 (1995).
10. Meloni, D., Laforge, S., Martin, D., Guisnet, M., Rombi, E., and Solinas, V., *Appl. Catal. A* **215**, 55 (2001).
11. Galli, E., Passaglia, E., and Zanazzi, P. F., *N. Jb. Miner. Mh.* **1982**, 1145 (1982).
12. Benco, L., Demuth, T., Hafner, J., and Hutschka, F., *J. Chem. Phys.* **111**, 7537 (1999).

13. Benco, L., Demuth, T., Hafner, J., and Hutschka, F., *Chem. Phys. Lett.* **324**, 373 (2000).
14. Benco, L., Demuth, T., Hafner, J., and Hutschka, F., *Chem. Phys. Lett.* **330**, 457 (2000).
15. Benco, L., Demuth, T., Hafner, J., and Hutschka, F., *Microporous Mesoporous Mater.* **42**, 1 (2001).
16. Benco, L., Demuth, T., Hafner, J., Hutschka, F., and Toulhoat, H., *J. Chem. Phys.* **114**, 6327 (2001).
17. Dura-Vila, V., and Gale, J. D., *J. Phys. Chem. B* **105**, 6158 (2001).
18. Corbató, C. E., Tettenhorst, R. T., and Cristoph, G. C., *Clays Clay Miner.* **33**, 71 (1985).
19. Jones, R. O., and Gunnarsson, O., *Rev. Mod. Phys.* **61**, 689 (1989).
20. Perdew, J. P., Chevary, A., Vosko, S. H., Jackson, K. A., Peredsen, M. R., Singh, D. J., and Fiolhais, C., *Phys. Rev. B* **46**, 6671 (1992).
21. Blöchl, P. E., *Phys. Rev. B* **50**, 17953 (1994).
22. Kresse, G., and Joubert, D., *Phys. Rev. B* **59**, 1758 (1999).
23. Vanderbilt, D., *Phys. Rev. B* **41**, 7892 (1990).
24. Kresse, G., and Hafner, J., *J. Phys. Condens. Matter* **6**, 8245 (1994).
25. Kresse, G., and Furthmüller, J., *Phys. Rev. B* **54**, 11169 (1996).
26. Nosé, S., *J. Chem. Phys.* **81**, 511 (1984).
27. Allen, M. P., and Tildesley, D. J., "Computer Simulations of Liquids." Clarendon, Oxford, 1987.
28. Benco, L., Tunega, D., Hafner, J., and Lischka, H., *J. Phys. Chem. B* **105**, 10812 (2001).
29. Demuth, T., Benco, L., Hafner, J., and Toulhoat, H., *Int. J. Quantum Chem.* **84**, 110 (2001).
30. Fleisch, T. H., Meyers, B. L., Ray, G. L., Hall, J. B., and Marshall, C. L., *J. Catal.* **99**, 117 (1986).